

# Surface Impedance Measurements on Nb<sub>3</sub>Sn in High Magnetic Fields

Andrea Alimenti, *Student Member, IEEE*, Nicola Pompeo, *Senior Member, IEEE*,  
Kostiantyn Torokhtii, *Member, IEEE* Tiziana Spina, René Flükiger, Luigi Muzzi, *Senior Member, IEEE*  
Enrico Silva, *Senior Member, IEEE*

**Abstract**—Nb<sub>3</sub>Sn is a superconductor of great relevance for perspective RF applications. We present for the first time surface impedance ( $Z_s$ ) measurements at 15 GHz and low RF field amplitude on Nb<sub>3</sub>Sn in high magnetic fields up to 12 T, with the aim of increasing the knowledge of Nb<sub>3</sub>Sn behavior in such conditions.  $Z_s$  is a fundamental material parameter that directly gives useful information about the dissipative and reactive phenomena when the superconductor is subjected to high-frequency excitations. Therefore, we present an analysis of the measured  $Z_s$  with the aim of extracting interesting data about pinning in Nb<sub>3</sub>Sn at high frequencies. From  $Z_s$  we extract the vortex motion complex resistivity to obtain the  $r$ -parameter and the depinning frequency  $\nu_p$  in high magnetic fields. The comparison of the results with the literature shows that the measured  $\nu_p$  on bulk Nb<sub>3</sub>Sn is several times greater than that of pure Nb. This demonstrates how Nb<sub>3</sub>Sn can be a good candidate for RF technological applications, also in high magnetic fields.

**Index Terms**—High magnetic fields, microwave, Nb<sub>3</sub>Sn, depinning frequency, surface impedance.

## I. INTRODUCTION

CURRENTLY Nb<sub>3</sub>Sn is the most interesting technological superconductor both for high performance dc applications like magnets for nuclear fusion or particle accelerators, and for potential radiofrequency applications as resonating cavities [1]–[6].

In applications like superconductive power cables in high magnetic fields, it is well known that vortex motion is the main contribution to the conduction losses. Hence, the experimental study of fluxons behavior, and their pinning, is of great relevance.

At radiofrequency (RF) and microwaves (mw), pinning is still a relevant topic, since vortices are much more free to dissipate. Challenging applications of Nb<sub>3</sub>Sn are represented by the RF accelerating cavities for particles accelerators [3], [7]. Nb cavities are currently being used but their technological limits seem to be reached [3], so to overcome their performances it is necessary to consider other superconductors and Nb<sub>3</sub>Sn is a potential candidate [8]. Nb<sub>3</sub>Sn offers approximately twice the critical temperature  $T_c$  and the superheating field  $H_{sh}$  with respect to Nb. This yields an improved cryogenic efficiency

and perspective higher accelerating fields [3]. However, it must be mentioned that to date, Nb<sub>3</sub>Sn cavities show a limit of peak surface magnetic field at  $\sim 70$  mT [3] which is still lower than the highest peak RF magnetic field reached with bulk Nb cavities  $\sim 209$  mT [9].

The improvement of the actual technological limits of this superconductor, in terms of critical current  $J_c$  and superheating field  $H_{sh}$ , is a mandatory requirement for the development of some of the presented applications. For this reason an in depth study of the RF electrodynamic response of Nb<sub>3</sub>Sn when subjected to extreme working conditions is needed.

For RF applications the depinning frequency  $\nu_p$  is the most relevant parameter because it marks the boundary between the frequency band where the response of fluxons to harmonic excitation is mainly elastic ( $\nu < \nu_p$ ) and the range where the vortex oscillation becomes purely dissipative ( $\nu > \nu_p$ ) [10]. The higher the  $\nu_p$  the higher the usable working frequencies are with a given SC with reduced dissipation.

Despite the relevance of Nb<sub>3</sub>Sn, to our knowledge no high magnetic fields microwave measurements are present in literature on Nb<sub>3</sub>Sn. In this work we present the first microwave characterization of Nb<sub>3</sub>Sn in high magnetic fields through  $Z_s$  measurements, performed with low RF field amplitude. From the  $Z_s$  analysis, the  $\nu_p$  is determined as a function of temperature  $T$ . We find that  $\nu_p$  attains values much larger than in Nb, thus making Nb<sub>3</sub>Sn an attractive material for its RF and mw potential performance in high magnetic fields.

The paper is organized as follows. In Sec.II we briefly recall the main model for  $Z_s$  in a superconductor in the vortex state. In Sec.III we describe the experimental setup and method. In Sec.IV we present the characterization of the sample and the experimental results for  $Z_s$ . Short conclusions are presented in Sec.V.

## II. SURFACE IMPEDANCE IN THE MIXED STATE

At high frequencies, the electromagnetic response of a conductor is modelled by the complex surface impedance  $Z_s$ . For bulk good conductors in the local limit and normal incidence electromagnetic waves, the surface impedance [11] is defined as  $Z_s = R_s + iX_s = \sqrt{i\omega\mu_0\tilde{\rho}} = i\omega\mu_0\tilde{\lambda}$ , where  $R_s$  and  $X_s$  are the surface resistance and reactance respectively,  $\omega$  the angular frequency,  $\mu_0$  the vacuum magnetic permeability and  $\tilde{\rho} = i\omega\mu_0\tilde{\lambda}^2$  the complex resistivity and  $\tilde{\lambda}$  a complex shielding length. The magnetic field  $H$  and temperature  $T$  dependence of  $\tilde{\lambda}$  models the dissipative and reactive phenomena of type-II superconductors: quasiparticle scattering and vortex flow,

A. Alimenti, N. Pompeo, K. Torokhtii and E. Silva are with the Department of Engineering, Università Roma Tre, 00146 Roma, Italy. Corresponding author: A. Alimenti; e-mail: andrea.alimenti@uniroma3.it.

T. Spina and R. Flükiger are with the European Organization for Nuclear Research (CERN), Technology Department, Geneva, Switzerland

L. Muzzi is with ENEA - Frascati Research Centre, Frascati, Italy

Manuscript received January 9, 2019.

as well as the pinning properties. As defined in [12],  $\tilde{\lambda}$  is a function of the complex conductivity  $\sigma_{2f} = \sigma_1 - i\sigma_2$  and of the vortex motion resistivity  $\rho_{vm}$  [13]. If  $\sigma_1 \ll \sigma_2$ , hence not too close to  $T_c$  and  $H_{c2}$ , one finds:

$$Z_s = i\omega\mu_0\sqrt{\lambda^2 - i\rho_{vm}/\omega\mu_0}, \quad (1)$$

where  $\lambda$  is the London penetration depth and  $\rho_{vm}$  is the vortex motion complex resistivity. If the applied magnetic field  $H = 0$  and  $T \rightarrow 0$  K, there are no fluxons in the SC, hence  $\rho_{vm} = 0$  and  $R_{s,ref} \sim 0$ ,  $X_{s,ref} = \omega\mu_0\lambda$ .

High-frequency microwave measurements are particularly interesting since at these frequencies the displacements of the fluxons from their equilibrium positions, due to the induced microwave (mw) currents ( $J_{mw}$ ), are so small that dynamic mutual interactions of fluxons can be discarded or reduced to an average effect. Thus,  $\rho_{vm}$  can be described by simplified, single-fluxon, local models such as the Gittleman-Roseblum (GR) model where one writes (having neglected thermal fluctuations) [10], [14]:

$$\rho_{vm} = \rho'_{vm} + i\rho''_{vm} = \rho_{ff} \frac{1}{1 - i\nu_p/\nu}, \quad (2)$$

with  $\rho_{ff}$  the flux-flow resistivity, and  $\nu_p$  appears explicitly.

Within the GR model the so called  $r$ -parameter, defined as  $r = \rho''_{vm}/\rho'_{vm}$ , gives immediately  $r = \nu_p/\nu$ , and thus  $\nu_p$  is directly obtained.

### III. EXPERIMENTAL TECHNIQUE

Dielectric loaded resonators offer high sensitivity for  $Z_s$  measurement [15]. In this technique the dielectric crystal, loaded into the cavity, is used to focus the electromagnetic (e.m.) field near the axis of the resonator, thus limiting the conduction losses. The higher the electrical permittivity of the crystal, the more the physical dimension of the resonator are reduced at the same working frequency, useful to probe small samples.

The sample is loaded into the cavity in order to substitute a base of the resonator (end-wall replacement configuration) [15]. We measure the changes in the quality factor  $Q$  and in the resonating frequency  $\nu_{res}$  with  $T$  or  $H$  due to the change in surface impedance of the superconducting sample.  $Q$  and  $\nu_{res}$  are obtained fitting the complex scattering parameters  $S_{12}(\nu)$  or  $S_{21}(\nu)$ .  $S_{11}(\nu)$  and  $S_{22}(\nu)$  are used to evaluate that the coupling factors of the 2-ports  $\beta_1 + \beta_2 = \beta < 0.01$  [15], firmly in the undercoupled regime, thus the measured quality factor  $Q_L = (1 + \beta)Q \simeq Q$ .

$Q$  and  $\nu_{res}$  yield  $R_s$  and  $X_s$  respectively, by means of the relation:

$$R_s + i\Delta X_s = \frac{G_s}{Q} - i2G_s \frac{\Delta\nu_{res}}{\nu_{res}} - background, \quad (3)$$

where  $G_s$  is a calculated geometrical factor,  $\Delta$  indicates a variation with respect to a reference value, and *background* indicates the (complex and  $T$ -dependent) contribution given by the resonator itself. A calibration of the resonator with a metallic sample allows to remove the background. Once the background is subtracted, the absolute values of  $Z_s(T, H)$  are obtained making use of the following fixed points: we set

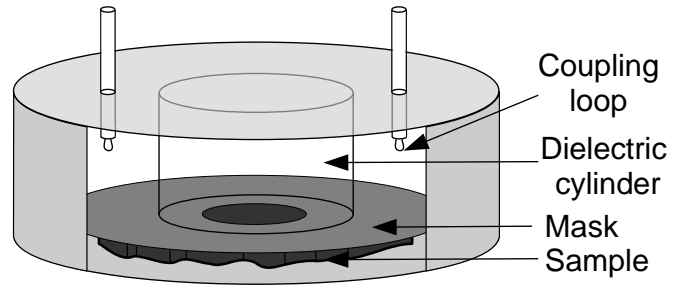


Fig. 1. Dielectric loaded resonator sketch. The metallic mask is used to keep the cylindrical symmetry despite the irregular shape of the sample. The resonating mode is excited with coaxial cables ended with magnetic loops. The dc magnetic field is perpendicular to the sample flat surface.

$R_s(H = 0, T \rightarrow 0) \sim 0$  (about this choice, see below for sensitivity comments) and  $R_s = X_s$  above  $T_c$  (real quasiparticle conductivity, Hagen-Rubens limit).

The specific dielectric resonator used here is of Hakki-Coleman type [16]. The sketch of the resonator is shown in Fig. 1. The entire assembly makes use of several springs in order to avoid issues related to the thermal expansions of the different components. The resonator works in transmission, and it is excited in the  $TE_{011}$  mode at  $\sim 14.9$  GHz with coaxial cables terminated with magnetic loops. A single-crystal sapphire cylindrical puck, 5.0 mm height and 8.0 mm diameter, loads the OFHC copper. Low dielectric losses ( $\tan \delta < 5 \cdot 10^{-8}$  at 9 GHz below 90 K) and relatively high permittivity ( $\epsilon_{\parallel} \simeq 11.5$ ,  $\epsilon_{\perp} \simeq 9.5$ ) [17] allows for negligible field density on the Cu walls. We note that the choice of Cu is dictated by the need to work in magnetic fields: superconducting cavities are ruled out. This constraint is detrimental to the sensitivity at low  $R_s$  values: our setup does not reach the sensitivity needed to assess the residual  $R_s$  at low temperature, but is instead suitable for the high- $R_s$  regime typical of the vortex motion.

The measurements are performed in helium flow by slowly raising the temperature (0.1 K/min) after Field Cooling (FC) to the lowest temperature (typically 6 K). The field  $H$  is applied perpendicular to the flat face of the sample.

Finally, in our experimental setup, the peak RF magnetic field amplitude parallel to the surface of the sample is assessed to be  $< 20 \mu\text{T}$ . The low RF field amplitude allows a characterization of the surface impedance in the linear regime where the  $Z_s$  does not depend on the power of the applied RF field [18]. It should be noted that the surface impedance in superconductors increases with the RF field amplitude [19] and in  $\text{Nb}_3\text{Sn}$  this trend is particularly accentuated (e.g. in  $\text{Nb}_3\text{Sn}$  the vortex dissipation due to the trapped field increases faster than what is observed in clean Nb) [19], [20].

### IV. RESULTS AND DISCUSSION

The flat polycrystalline bulk  $\text{Nb}_3\text{Sn}$  sample, of approximate dimensions  $7 \text{ mm} \times 5 \text{ mm}$ , and 1 mm thick, was obtained by sintering Nb and Sn powder (25 at.%Sn) mixture under an Argon pressure of 2 kbar at 1250 °C in Hot Isostatic Pressure (HIP) conditions. Through X-ray diffraction methods (Rietveld refinement), the long-range order parameter  $S$  was measured,

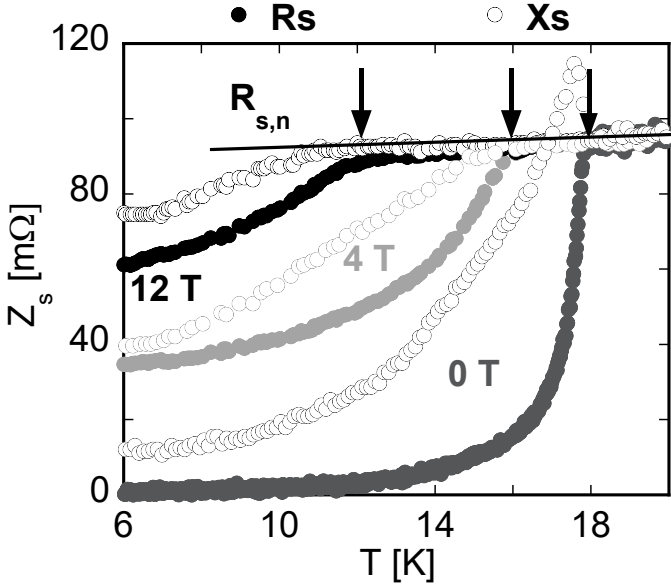


Fig. 2.  $Z_s$  measured at fixed  $\mu_0 H$ , depicted in the figure, and varying  $T$ . Full circles:  $R_s$ ; empty circles:  $X_s$ . Colors: black,  $\mu_0 H = 12$  T; light gray,  $\mu_0 H = 4$  T; dark gray,  $\mu_0 H = 0$  T. Vertical arrows indicate  $T_{c2}(H)$ .

showing a state of atomic ordering close to perfect ordering ( $S = 0.98 \pm 0.02$ ) [21].

In order to check the consistency of the data on our samples with the literature, we derived the normal state resistivity from the  $\text{Nb}_3\text{Sn}$  surface resistance  $R_{s,n}$  measured above  $T_c$  (see Fig.2):  $\rho_n = 2R_{s,n}^2/\omega\mu_0 = 14.8 \mu\Omega\text{cm}$ . The measured  $\rho_n$  is typical of  $\text{Nb}_3\text{Sn}$  samples with  $S = 0.97$  and 25 at.%Sn [22], [23], entirely consistent with our results [21]. The penetration depth  $\lambda(0) = X_s(H = 0, T \rightarrow 0)/\omega\mu_0 \sim 100$  nm is evaluated by extrapolating  $X_s(\mu_0 H = 0$  T) at low temperature. The obtained value is in fair agreement with reported data [24].

The  $\text{Nb}_3\text{Sn}$  surface impedance, measured in FC at  $\mu_0 H = \{0, 4, 12\}$  T, is shown in Fig.2. The beginning of the resistive transitions as a function of  $T$  and  $H$  are highlighted by the vertical arrows. We found that the behavior of the so-obtained  $H_{c2}(T)$  is perfectly linear, and we estimate the derivative of the upper critical field  $H_{c2}$  near  $T_c$ ,  $\mu_0 dH_{c2}/dT = 2.03$  T/K. The obtained value is fully consistent with literature [25].

Fig. 2 reports the set of measurements of  $Z_s(T, H)$ . The data do not present anomalous features. It can be deduced already from the raw data that the depinning frequency is of the same order of magnitude of the measuring frequency. In fact, the increases of  $R_s$  and  $X_s$  with the field are different, although not much. Recalling (1), (2), one see that for both  $\nu \ll \nu_p$  and  $\nu \gg \nu_p$ , the increase of  $R_s$  and  $Z_s$  should be the same. We then focus on the variations  $\Delta Z_s = Z_s - Z_s(H = 0)$  in the temperature range  $T/T_c \lesssim 0.8$ , in order to avoid the high- $T$  region, where thermal effects introduce additional phenomena and then model parameters. We note in passing that working with the differences allows to alleviate the potential issues concerning the sensitivity of the resonant frequency to thermal expansion. We set, consistent with our results,

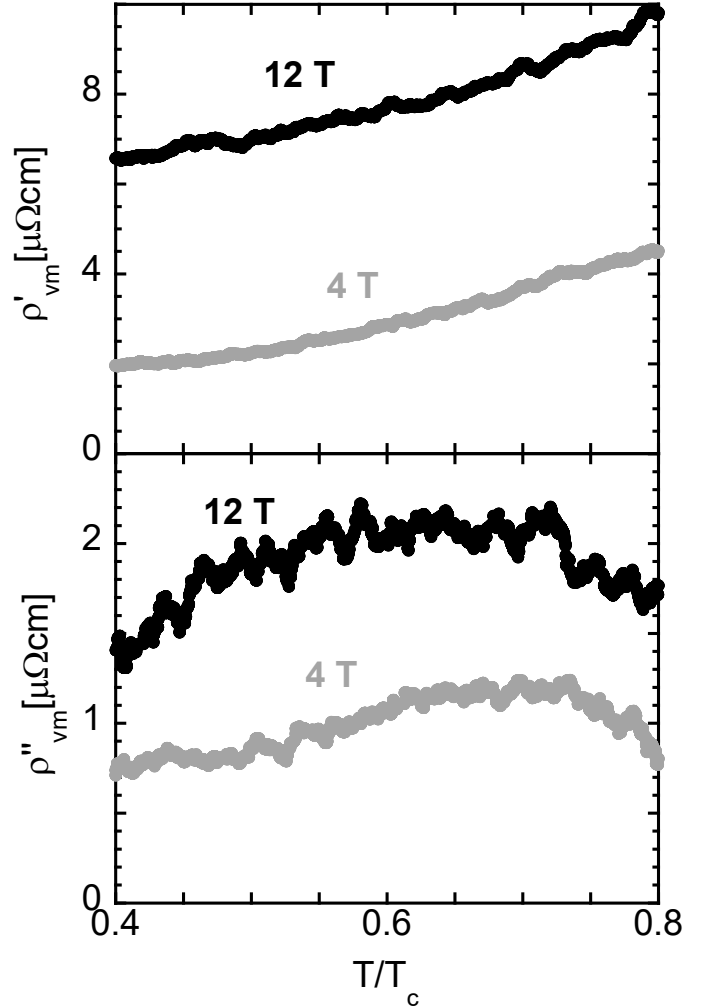


Fig. 3. The vortex motion resistivity  $\rho_{vm} = \rho'_{vm} + i\rho''_{vm}$  obtained by the  $\Delta Z_s$ . In the upper plot  $\rho'_{vm}$  and in the lower  $\rho''_{vm}$ . The black curves are measured at  $\mu_0 H = 12$  T while the gray at  $\mu_0 H = 4$  T.

$\lambda(T) = \lambda_0/\sqrt{1 - (T/T_c)^4}$ , and then from  $\Delta Z_s$  we isolate  $\Re(\rho_{vm}) = \rho'_{vm}$  and  $\Im(\rho_{vm}) = \rho''_{vm}$ . The vortex motion complex resistivity is reported in Fig. 3. It is clearly seen that  $\rho'_{vm} > \rho''_{vm}$ , although the latter is non negligible. It can be also observed that  $\rho''_{vm}$  shows a tendency to decrease at high  $T$ : this is completely reasonable, since at  $T_c$  one has no imaginary part in the resistivity. Accordingly,  $\rho'_{vm}$  steadily increases with  $T$ . We recall that, should it be pure flux-flow (no imaginary part), the well-known Bardeen-Stephen model [26] predicts  $\rho'_{vm} \propto (T_c - T)^{-1}$ , consistent with our data.

From (2) we directly derive  $\nu_p$  from the data in Fig. 3. The data for  $\nu_p$  are reported in Fig. 4. We immediately note that the values for  $\nu_p$  are quite large, ranging at low  $T$  from  $\sim 6$  GHz at 4 T to 4 GHz at 12 T. These values compare very favourably to Nb. In pure Nb films  $\nu_p$  rises with the decrease of film thickness, up to  $\nu_p \sim 20$  GHz in 10 nm film in 0.2 T perpendicular field, but it sharply falls down to 1 GHz in 160 nm films at 5 K [27]. It can be deduced that  $\nu_p$  in thick Nb films or bulks lays at best at 1 GHz, and more likely, well below. A second relevant aspect is the field resilience exhibited by  $\text{Nb}_3\text{Sn}$ :  $\nu_p$  is in the

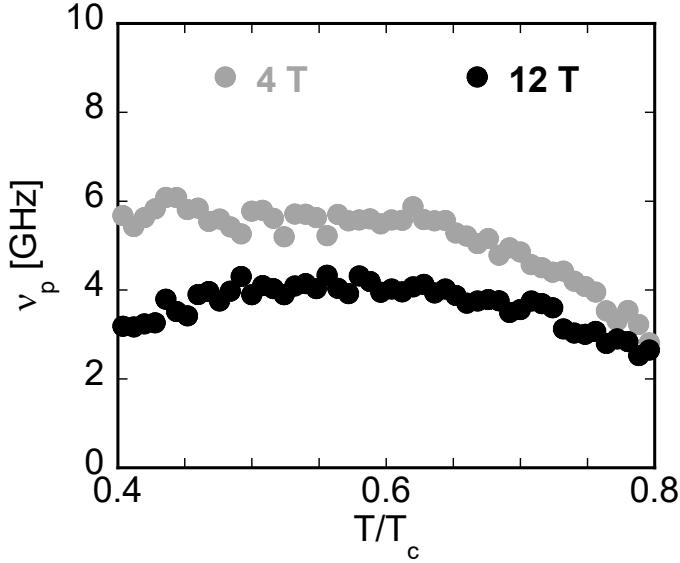


Fig. 4. The depinning frequency  $\nu_p$  at  $\mu_0 H = 12$  T (black points) and at  $\mu_0 H = 4$  T (gray points). The  $\nu_p$  is almost constant up to  $0.65 T_c$ .

several GHz range in fields as high as 12 T, so that  $\nu_p$  at 12 T in bulk Nb<sub>3</sub>Sn  $\nu_p$  is almost 5 times that of Nb thin film (thickness 160 nm) below 1 T, demonstrating enhanced Nb<sub>3</sub>Sn RF behavior with respect to elementary Nb thin films [27]–[29]. Further improvements on Nb<sub>3</sub>Sn  $\nu_p$  are realistically reachable with Nb<sub>3</sub>Sn thin films, where  $\nu_p$  is expected to rise in analogy to Nb, opening interesting possibilities of Nb<sub>3</sub>Sn applications at microwave frequencies. In order to complete the comparison with other superconductors, we note that a comparable depinning frequency (5 GHz) is exhibited by 13  $\mu\text{m}$  thickness foils of Pb<sub>0.83</sub>In<sub>0.17</sub> at 1.7 K and  $0.5 H_{c2}$  [10]. Cuprates are known to have large depinning frequency [30], [31], with high values in YBa<sub>2</sub>Cu<sub>3</sub>O<sub>7-x</sub> (YBCO) single crystal, about  $\nu_p \sim 20$  GHz at 45 K [30], [31]. YBCO thin films with BaZrO<sub>3</sub> columnar and elongated defects exhibits still enhanced pinning frequencies:  $\nu_p \sim 50$  GHz at 70 K [32]. However, it must be mentioned that, at least in Tl<sub>2</sub>Ba<sub>2</sub>Ca<sub>2</sub>CuO<sub>8+x</sub>, such high  $\nu_p$  are anomalously accompanied by a very large dissipation [33].

We make a final note on the possible effects of thermal activation (flux-creep). Should it be present, the effect is to reduce  $\rho''_{vm}$  and to increase  $\rho'_{vm}$ : the more the thermal creep is prominent the more the pinning effect vanishes and  $\rho_{vm} \rightarrow \rho_{ff}$  [12], [14]. From (2) and measurement frequency  $\nu > \nu_p$ , it can be shown that this phenomenon is modeled as a first approximation with a lowering of  $\nu_p$  in (2) in order to obtain the same creep-induced increase in  $\rho'_{vm}$  and reduction of  $\rho''_{vm}$ . Thus within this model, the obtained  $\nu_p$  is at worst an underestimate. For this reason, we can state that our measurements set a lower limit to the Nb<sub>3</sub>Sn depinning frequency (Fig. 4) without the need for entering any other parameter (i.e. the creep factor). Therefore, this result is robust against the possible presence of flux-creep: the depinning frequency remains rather high in Nb<sub>3</sub>Sn, much higher than in Nb.

## V. CONCLUSION

We presented the first microwave ( $\sim 15$  GHz) characterization of Nb<sub>3</sub>Sn in high magnetic fields (up to 12 T). The Nb<sub>3</sub>Sn surface impedance  $Z_s$  was evaluated in the mixed state to obtain information about the dissipative and reactive phenomena of vortex motion. From  $Z_s$  elaborations we obtained and showed the vortex motion complex resistivity, a quantity that directly allowed us to obtain the depinning frequency  $\nu_p$  of Nb<sub>3</sub>Sn. The depinning frequency is a parameter of great relevance because it establishes the frequency above which the elastic RF vortex motion becomes purely resistive. Hence,  $\nu_p$  is the highest theoretical working frequency for low loss RF applications in high magnetic fields.

The measured  $\nu_p$  is almost constant in temperature (up to  $0.65 T_c$ ) and decreases from 6.0 GHz at 4 T, to 4.5 GHz at 12 T. This result shows that the Nb<sub>3</sub>Sn exhibits much better RF characteristics than Nb and encourages the use of Nb<sub>3</sub>Sn in technological RF and mw applications up to few GHz also in presence of dc magnetic fields.

## REFERENCES

- [1] X. Xu, "A review and prospects for Nb<sub>3</sub>Sn superconductor development," *Supercond. Sci. Technol.*, vol. 30, no. 9, p. 093001, Aug 2017.
- [2] R. J. Thome, I. J. Central, and H. Teams, "Design & development of the ITER magnet system," *Cryogenics*, vol. 34, pp. 39–46, May. 1994.
- [3] S. Posen and D. L. Hall, "Nb<sub>3</sub>Sn superconducting radiofrequency cavities: fabrication, results, properties, and prospects," *Supercond. Sci. Technol.*, vol. 30, no. 3, p. 033004, Jan. 2017.
- [4] A. M. Valente-Feliciano, "Superconducting RF materials other than bulk niobium: a review," *Supercond. Sci. Technol.*, vol. 29, no. 11, p. 113002, Sep. 2016.
- [5] H. Padamsee, J. Knobloch, and T. Hays, *RF Superconductivity for Accelerators*. Wiley-VCH, 1998.
- [6] R. Flükiger, "Overview of superconductivity and challenges in applications," *Rev. Accel. Sci. Technol.*, vol. 5, pp. 1–23, Apr. 2012.
- [7] H. Padamsee, *RF superconductivity: science, technology, and applications*. John Wiley & Sons, 2009.
- [8] C. Becker, S. Posen *et al.*, "Analysis of Nb<sub>3</sub>Sn surface layers for superconducting radio frequency cavity applications," *Appl. Phys. Lett.*, vol. 106, no. 8, p. 082602, Feb. 2015.
- [9] A. Grassellino, A. Romanenko *et al.*, "Accelerating fields up to 49 MV/m in TESLA-shape superconducting RF niobium cavities via 75C vacuum bake," *arXiv preprint arXiv:1806.09824*, Jun. 2018.
- [10] J. I. Gittleman and B. Rosenblum, "Radio-frequency resistance in the mixed state for subcritical currents," *Phys. Rev. Lett.*, vol. 16, no. 17, p. 734, Apr. 1966.
- [11] R. E. Collin, *Foundations for microwave engineering*. John Wiley & Sons, 2007.
- [12] M. W. Coffey and J. R. Clem, "Unified theory of effects of vortex pinning and flux creep upon the RF surface impedance of type-II superconductors," *Phys. Rev. Lett.*, vol. 67, no. 3, p. 386, 1991.
- [13] M. Tinkham, *Introduction to superconductivity*. Courier Corporation, 1996.
- [14] N. Pompeo and E. Silva, "Reliable determination of vortex parameters from measurements of the microwave complex resistivity," *Phys. Rev. B*, vol. 78, no. 9, p. 094503, Sep. 2008.
- [15] L.-F. Chen, C. Ong *et al.*, *Microwave electronics: measurement and materials characterization*. John Wiley & Sons, 2004.
- [16] B. Hakki and P. Coleman, "A dielectric resonator method of measuring inductive capacities in the millimeter range," *IRE Trans. Microwave Theory and Tech.*, vol. 8, no. 4, pp. 402–410, Sep. 1960.
- [17] V. Braginsky, V. Ilchenko, and K. S. Bagdassarov, "Experimental observation of fundamental microwave absorption in high-quality dielectric crystals," *Phys. Lett. A*, vol. 120, no. 6, pp. 300–305, Mar. 1987.
- [18] H. Weinstock and M. Nisenoff, *Microwave superconductivity*. Springer Science & Business Media, 2012, vol. 375.
- [19] M. Martinello, A. Grassellino *et al.*, "Effect of interstitial impurities on the field dependent microwave surface resistance of niobium," *Appl. Phys. Lett.*, vol. 109, no. 6, p. 062601, Aug. 2016.

- [20] D. Hall, J. Kaufman *et al.*, “First results from new single-cell Nb<sub>3</sub>Sn cavities coated at Cornell University,” in *Proc. of International Particle Accelerator Conference (IPAC'17)*, May 2017, pp. 40–43.
- [21] T. Spina, *Proton irradiation effects on Nb<sub>3</sub>Sn wires and thin platelets in view of High Luminosity LHC upgrade*. Ph.D thesis in Physics, Universite de Geneve, Departement de Physique de la Matiere Quantique (DQMP), 2015.
- [22] R. Flukiger, H. Kupfer *et al.*, “Effect of atomic ordering and composition changes on the electrical resistivity of Nb<sub>3</sub>Al, Nb<sub>3</sub>Sn, Nb<sub>3</sub>Ge, Nb<sub>3</sub>Ir, V<sub>3</sub>Si and V<sub>3</sub>Ga,” *IEEE Trans. Magn.*, vol. 23, no. 2, pp. 980–983, Mar. 1987.
- [23] A. Godeke, “A review of the properties of Nb<sub>3</sub>Sn and their variation with A15 composition, morphology and strain state,” *Supercond. Sci. Technol.*, vol. 19, no. 8, p. R68, Jun. 2006.
- [24] Y. Li and Y. Gao, “GLAG theory for superconducting property variations with A15 composition in Nb<sub>3</sub>Sn wires,” *Sci. Rep.*, vol. 7, no. 1, p. 1133, Apr. 2017.
- [25] T. P. Orlando, E. J. McNiff *et al.*, “Critical fields, Pauli paramagnetic limiting, and material parameters of Nb<sub>3</sub>Sn and V<sub>3</sub>Si,” *Phys. Rev. B*, vol. 19, pp. 4545–4561, May. 1979.
- [26] J. Bardeen and M. J. Stephen, “Theory of the motion of vortices in superconductors,” *Phys. Rev.*, vol. 140, pp. A1197–A1207, Nov. 1965.
- [27] D. Janjušević, M. S. Grbić *et al.*, “Microwave response of thin niobium films under perpendicular static magnetic fields,” *Phys. Rev. B*, vol. 74, no. 10, p. 104501, Sep. 2006.
- [28] N. Pompeo, K. Torokhtii *et al.*, “Superconducting and Structural Properties of Nb/PdNi/Nb Trilayers,” *J. Supercond. Novel Magn.*, vol. 26, no. 5, pp. 1939–1943, May. 2013.
- [29] E. Silva, N. Pompeo, and S. Sarti, “Wideband microwave measurements in Nb/Pd<sub>84</sub>Ni<sub>16</sub>/Nb structures and comparison with thin Nb films,” *Supercond. Sci. Technol.*, vol. 24, no. 2, p. 024018, Jan. 2011.
- [30] M. Golosovsky, M. Tsindlekht, and D. Davidov, “High-frequency vortex dynamics in YBa<sub>2</sub>Cu<sub>3</sub>O<sub>7</sub>,” *Supercond. Sci. Technol.*, vol. 9, no. 1, p. 1, Sep. 1996.
- [31] Y. Tsuchiya, K. Iwaya *et al.*, “Electronic state of vortices in YBa<sub>2</sub>Cu<sub>3</sub>O<sub>y</sub> investigated by complex surface impedance measurements,” *Phys. Rev. B*, vol. 63, no. 18, p. 184517, Apr. 2001.
- [32] K. Torokhtii, N. Pompeo *et al.*, “Measurement of vortex pinning in YBCO and YBCO/BZO coated conductors using a microwave technique,” *IEEE Trans. Appl. Supercond.*, vol. 26, no. 3, p. 8001605, Apr. 2016.
- [33] N. Pompeo, H. Schneidewind, and E. Silva, “Measurements of microwave vortex response in dc magnetic fields in Tl<sub>2</sub>Ba<sub>2</sub>CaCu<sub>2</sub>O<sub>8+x</sub> films,” presented at ASC 2018, abstract no. 2985707, submitted for publication.